DOI: 10.1002/ejic.200700657

Homo- and Heterometallic Coordination Oligomers and Polymers Derived from the Preformed Complexes $[Cu(bdmpp)(MeCN)_2](ClO_4)_2$, $[Cu(bdmpp)(N_3)_2]$, and $[Cu(bdmpp)(N_3)(\mu\text{-}N_3)]_2$ [bdmpp = 2,6-bis(3,5-dimethyl-1*H*-pyrazol-1-yl)pyridine]: Syntheses, Structures, and Redox Properties

Guang-Fei Liu,[a] Zhi-Gang Ren,[a] Hong-Xi Li,[a] Yang Chen,[a] Qiu-Hong Li,[a] Yong Zhang,[a] and Jian-Ping Lang*[a,b]

Keywords: Copper / Structures / Oligomers / Polymers / Redox properties

Reactions of three Cu^{II} complexes of 2,6-bis(3,5-dimethyl-1*H*-pyrazol-1-yl)pyridine (bdmpp), $[Cu(bdmpp)(MeCN)_2](ClO_4)_2$ (**1**), $[Cu(bdmpp)(N_3)_2]\cdot 1.5H_2O$ (**2**·$1.5H_2O$), and $[Cu(bdmpp)(N_3)(\mu\text{-}N_3)]_2\cdot 2MeOH$ (**3**·2MeOH), with 4,4′-bipy, dicyanamide (dca), azide, and MCl_2 (M = Cu, Co, Ni) yield a series of homo- and heterometallic coordination oligomers and polymers, $[\{Cu(bdmpp)(ClO_4)\}_2(\mu\text{-}4,4'\text{-bipy})](ClO_4)_2$ (**4**), $\{[Cu(bdmpp)(\mu\text{-dca})](ClO_4)\}_n$ (**5**), $\{[Cu(bdmpp)(\mu\text{-}N_3)](ClO_4)\cdot MeCN\}_n$ (**6**), $[\{Cu(N_3)(bdmpp)\}_2(\mu\text{-}N_3)_2Cu(N_3)_2]$ (**7**), and $[\{Cu(\mu\text{-}N_3)(bdmpp)(\mu\text{-}N_3)M(\mu\text{-}N_3)(X)\}_2\cdot eMeCN]_n$ (**8**: M = Co, X = N_3, *e* = 0; **9**: M = Ni, X = Cl; *e* = 4). Compounds **1**–**9** have been characterized by elemental analysis, IR spectroscopy, and single-crystal X-ray crystallography. Compound **4** has a centrosymmetric dimeric dication structure in which two $[Cu(bdmpp)(ClO_4)]^+$ fragments are bridged by one 4,4′-bipy. Compounds **5** and **6** have a 1D linear or spiral chain extending along the *b* axis in which each $[Cu(bdmpp)]^{2+}$ fragment is linked through bridging dca or azide anions, respectively. Compound **7** has a trinuclear sandwich structure in which two molecules of **2** link a $Cu(N_3)_2$ species through two end-on bridging azide anions. Compounds **8** and **9** have a similar 1D chain structure extending along the *c* axis in which $[Cu(\mu\text{-}N_3)(bdmpp)(\mu\text{-}N_3)M(\mu\text{-}N_3)(X)]_2$ (M = Co, Ni) molecules are linked by end-to-end azide anions (**8**) or end-on azide anions (**9**). In addition, the electrochemical properties of **1**–**9** in DMF were investigated by cyclic voltammetry. (© Wiley-VCH Verlag GmbH & Co. KGaA, 69451 Weinheim, Germany, 2007)

Introduction

In past decades, design and construction of coordination oligomers and polymers from metal complex or cluster precursors has attracted considerable attention because of their structural diversity[1–11] and their potential applications in advanced materials.[12–20] From the viewpoint of the "design", a suitable metal complex or cluster precursor may possess one of the following requirements. Firstly, that some ligands around the metal center or cluster core are labile and readily replaced by other strong donor ligands. Secondly, that some ligands in the complex or cluster are potential multilinkers to interconnect with other metal centers or cluster cores. Thirdly, that the coordination is unsaturated for at least one metal atom of the complex or cluster. Many preformed clusters match these requirements and have been employed to serve as excellent precursors for the formation of a number of cluster-based supramolecules.[3–6,8–11,21–24] In contrast to the cluster precursors, employment of the preformed metal complexes for the formation of homo- or heterometallic coordination oligomers or polymers is less explored.

Recently we have been engaged in the construction of coordination oligomers and polymers from preformed mononuclear complexes and metal sulfide clusters.[11,21–26] One useful approach is to introduce the bulky ligands that block some of the coordination sites of the metal center, which may cause it to form the unsaturated coordination geometry. Among numerous bulky ligands, the tridentate ligand 2,6-bis(3,5-dimethyl-1*H*-pyrazol-1-yl)pyridine (bdmpp) attracted our attention. This ligand has been employed to react with metal ions to form various complexes.[27–30] Some metal/bdmpp complexes did show unsaturated coordination geometry around the metal center.[27–30] However, these compounds have not been used as precursors to further assemble coordination oligomers and polymers. To this end, we prepared three Cu^{II}/bdmpp complexes, $[Cu(bdmpp)(MeCN)_2](ClO_4)_2$ (**1**), $[Cu(bdmpp)(N_3)_2]\cdot 1.5H_2O$ (**2**·$1.5H_2O$), and $[Cu(bdmpp)(N_3)(\mu\text{-}N_3)]_2\cdot 2MeOH$ (**3**·2MeOH), in high yields. Compounds **1**–**3** match the above-mentioned requirements and could be used as pre-

[a] School of Chemistry and Chemical Engineering, Suzhou University,
Suzhou 215123, Jiangsu, People's Republic of China
Fax: +86-512-65880089
E-mail: jplang@suda.edu.cn
[b] State Key Laboratory of Coordination Chemistry, Nanjing University,
Nanjing 210093, Jiangsu, People's Republic of China

cursors to form a family of homo- and heterometallic coordination oligomers and polymers: $[\{Cu(bdmpp)(ClO_4)\}_2(\mu\text{-}4,4'\text{-bipy})](ClO_4)_2$ (**4**), $\{[Cu(bdmpp)(\mu\text{-dca})](ClO_4)\}_n$ (**5**), $\{[Cu(bdmpp)(\mu\text{-}N_3)](ClO_4)\cdot MeCN\}_n$ (**6**), $[\{Cu(N_3)(bdmpp)\}_2(\mu\text{-}N_3)_2Cu(N_3)_2]$ (**7**), and $[\{Cu(\mu\text{-}N_3)(bdmpp)(\mu\text{-}N_3)M(\mu\text{-}N_3)(X)\}_2\cdot e MeCN]_n$ (**8**: M = Co, X = N_3, e = 0; **9**: M = Ni, X = Cl; e = 4). Furthermore, we have employed cyclic voltammetry (CV) to investigate the electrochemical behaviors of **1**–**9** in order to understand the changes of the redox properties of the assembled oligomers and polymers relative to their precursors. In this paper, we report their syntheses, crystal structures, and redox properties.

Results and Discussion

Reaction of $[Cu(MeCN)_4](ClO_4)_2$ with equimolar bdmpp in MeCN resulted in a green solution. Slow diffusion of Et_2O into the solution led to the formation of green blocks of **1** in 85% yield (Scheme 1). On the other hand, treatment of $CuCl_2\cdot 2H_2O$ with NaN_3 and bdmpp in 1:2:1 and 1:4:1 (molar ratio) in MeOH followed by slow evaporation of solvents gave rise to **2**·1.5H_2O and **3**·2MeOH in 75% and 72% yields, respectively. The formation of **2**·1.5H_2O and **3**·2MeOH depended on the molar ratio of $CuCl_2\cdot 2H_2O$ and NaN_3 during the reaction. As discussed later in this paper, when the lower ratio (1:2) was used, the Cu atom was apt to adopt a less saturated coordination (five-coordinate) and **2**·1.5H_2O was thus formed. When the higher ratio (1:4 or more) was used, the Cu atom was more apt to adopt a saturated coordination (six-coordinate) and **3**·2MeOH was formed.

As discussed later in this paper, the Cu^{II} atom in **1** is chelated by one bdmpp and coordinated by two labile MeCN molecules. When the two MeCN molecules are replaced by strong bridging donor ligands, the Cu^{II} center may have up to three more coordination sites available and its trigonal-bipyramidal coordination geometry may be turned to square-planar, square-pyramidal, or octahedral. The remaining $[Cu(bdmpp)]^{2+}$ fragment along with bridging ligands may serve as multiconnecting nodes to form novel oligomers and polymers. Among the potential bridging donor ligands, we chose 4,4′-bypyridine (4,4′-bipy), sodium dicyanamide, and sodium azide for this purpose.

Treatment of **1** with equimolar 4,4′-bipy followed by a similar procedure used in the isolation of **1** produced blue crystals of **4** in 63% yield, while reactions of **1** with equimolar sodium dicyanamide or sodium azide followed by a similar workup gave rise to green crystals of **5** and deep green crystals of **6** in 75% and 80% yields, respectively (Scheme 1). It is noted that in these cases, the two MeCN molecules coordinated at the Cu center of **1** were replaced and the $[Cu(bdmpp)]^{2+}$ fragment was retained, even though the coordination geometry of the Cu atom was changed during the reactions. The different outcomes from the aforementioned three reactions deserve comment. Compared with the dca and N_3^- ligands, 4,4′-bipy seems somewhat bulky and rigid. The replacement of the two MeCN molecules of the cation of **1** by 4,4′-bipy only afforded a dinuclear complex **4**. The less rigid ligand, dca or N_3^-, removed the two MeCN molecules of the cation of **1** and linked the $[Cu(bdmpp)]^{2+}$ fragments through end-to-end μ-1,5-bridging mode (dca) or μ-1,3-bridging mode (N_3^-), forming polymeric species **5** and **6**, respectively.

In the cases of **2** and **3**, both complexes may also work as precursors for oligomers and polymers as they have two terminal azides that could link other metal ions. Accordingly, reactions of **2** with a mixture of $CuCl_2\cdot 2H_2O$ and NaN_3 in a molar ratio of 1:1:4 produced the homometallic

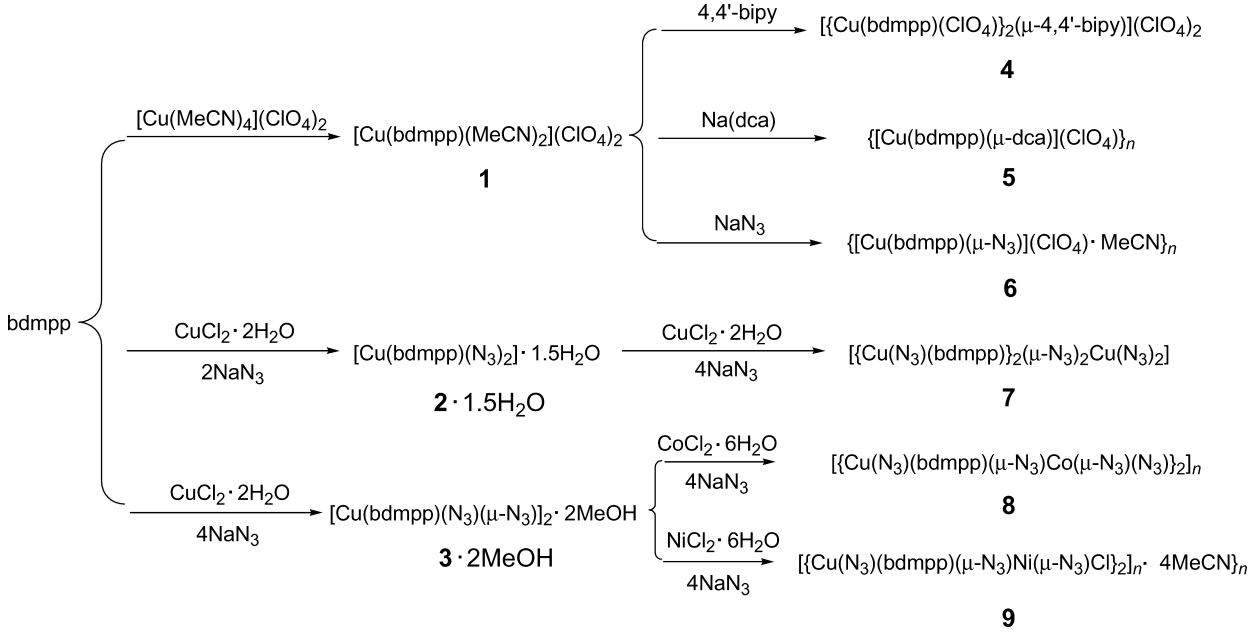

Scheme 1. Reactions of bdmpp with $[Cu(MeCN)_4](ClO_4)_2$ and $CuCl_2\cdot 2H_2O/NaN_3$; reactions of **1** with 4,4′-bipy, Na(dca), and NaN_3; reactions of **2** with $CuCl_2\cdot 2H_2O$ and NaN_3; and reactions of **3** with $MCl_2\cdot 6H_2O$ (M = Cu, Co, Ni) and NaN_3.

oligomer **7** in 67% yield, while those of **3** with a mixture of $MCl_2·6H_2O$ (M = Co, Ni) and NaN_3 in a molar ratio of 1:1:4 followed by a similar workup afforded two heterometallic polymers, **8** and **9**, in 50% and 49% yields, respectively (Scheme 1). In these cases, **2** or **3** only used their terminal azides to link the possible $Cu(N_3)_2$ or $[M(\mu\text{-}N_3)(X)]_2$ (M = Co, X = N_3; M = Ni, X = Cl) species. The coordination geometry for each Cu center in **2** or **3** is retained.

Solids **1**–**9** were relatively air- and moisture-stable, and were soluble in DMF and DMSO. The elemental analysis was consistent with the chemical formula of **1**–**9**. The IR spectrum of **1** showed a sharp ν(CN) at 2249 cm^{-1}, suggesting the presence of terminal acetonitrile molecules. In the IR spectra of **2**·1.5H_2O, **3**·2MeOH, and **6**–**9** the strong absorptions at 2040/2068 (**2**·1.5H_2O), 2045 (**3**·2MeOH), 2041 (**7**), and 2029 (**8**) cm^{-1} may be attributed to the asymmetric stretching frequencies of the terminal azide groups while those at 2073 (**3**·2MeOH), 2054/2066 (**6**), 2066 (**7**), 2066 (**8**), and 2069 (**9**) cm^{-1} may be assigned to be the asymmetric stretching vibrations of end-on or end-to-end bridging azide groups.[31] In the IR spectrum of **5**, a band at 2179 cm^{-1} was assigned to be the stretching vibration of the dca ligand with a bidentate $\mu_{1,5}$ coordination.[25] In the IR spectra of **1** and **4**–**6**, strong and broad peaks at 1122/1087/1060 (**1**), 1093/1024 (**5**), and 1144/1118/1084 (**6**) cm^{-1} are the characteristic Cl–O stretching vibrations of the free perchlorate anions while that at 1087 cm^{-1} (**4**) may be assigned to be a unidentate perchlorato ligand. The identities of **1**–**9** were further confirmed by X-ray crystallography.

Compound **1** crystallizes in the orthorhombic space group *Pbca* and the asymmetric unit consists of one $[Cu(bdmpp)(MeCN)_2]^{2+}$ dication and two ClO_4^- anions. Unlike the most reported fashion of the square-pyramidal geometry,[30] the five-coordinate copper(II) atom in **1** adopts a distorted trigonal-bipyramidal geometry, which is coordinated by three N atoms from the bdmpp ligand and two N atoms from the acetonitrile molecules (Figure 1). N(1) and N(5) are located in apical positions, while N(3),

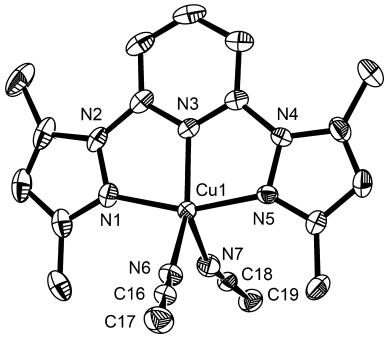

Figure 1. Perspective view of the $[Cu(bdmpp)(MeCN)_2]^{2+}$ dication of **1** with 50% thermal ellipsoids. All hydrogen atoms are omitted for clarity.

Table 1. Selected bond lengths [Å] and angles [°] of **1**–**3**.[a]

	Compound **1**		
Cu(1)–N(1)	1.981(3)	Cu(1)–N(6)	2.054(3)
Cu(1)–N(3)	1.947(2)	Cu(1)–N(7)	2.162(3)
Cu(1)–N(5)	1.967(2)		
N(1)–Cu(1)–N(3)	78.95(10)	N(5)–Cu(1)–N(6)	97.30(10)
N(3)–Cu(1)–N(5)	79.52(10)	N(1)–Cu(1)–N(7)	97.72(10)
N(5)–Cu(1)–N(1)	158.43(11)	N(3)–Cu(1)–N(7)	122.33(10)
N(1)–Cu(1)–N(6)	98.58(10)	N(5)–Cu(1)–N(7)	94.80(10)
N(3)–Cu(1)–N(6)	140.88(10)	N(6)–Cu(1)–N(7)	96.77(11)
	Compound **2**		
Cu(1)–N(1)	2.0192(19)	Cu(1)–N(6)	1.9373(18)
Cu(1)–N(3)	1.9721(17)	Cu(1)–N(9)	2.186(2)
Cu(1)–N(5)	2.0124(19)		
N(1)–Cu(1)–N(3)	78.09(7)	N(6)–Cu(1)–N(9)	102.39(9)
N(3)–Cu(1)–N(5)	78.37(8)	N(1)–Cu(1)–N(6)	100.50(8)
N(5)–Cu(1)–N(1)	156.18	N(3)–Cu(1)–N(6)	152.30(7)
N(3)–Cu(1)–N(9)	105.27(8)	N(5)–Cu(1)–N(6)	98.62(8)
N(5)–Cu(1)–N(9)	93.64(9)	N(1)–Cu(1)–N(9)	95.98(9)
	Compound **3**		
Cu(1)–N(1)	2.090(4)	Cu(1)–N(9)	2.107(5)
Cu(1)–N(3)	2.021(4)	Cu(1)–N(6A)	2.149(4)
Cu(1)–N(5)	2.096(4)	Cu(1)–N(6)	2.038(4)
N(1)–Cu(1)–N(3)	77.42(16)	N(5)–Cu(1)–N(9)	91.19(17)
N(3)–Cu(1)–N(5)	76.80(15)	N(6)–Cu(1)–N(9)	95.50(17)
N(5)–Cu(1)–N(1)	153.63(16)	N(1)–Cu(1)–N(6A)	92.54(16)
N(1)–Cu(1)–N(6)	102.65(16)	N(3)–Cu(1)–N(6A)	88.57(15)
N(3)–Cu(1)–N(6)	166.20(16)	N(5)–Cu(1)–N(6A)	92.26(15)
N(5)–Cu(1)–N(6)	103.70(16)	N(6)–Cu(1)–N(6A)	77.63(17)
N(1)–Cu(1)–N(9)	87.10(17)	N(9)–Cu(1)–N(6A)	172.88(17)
N(3)–Cu(1)–N(9)	98.28(17)		

[a] Symmetry code: A: $-x$, $-y + 2$, $-z$.

N(6), and N(7) are in equatorial positions. The two Cu–N (MeCN) bonds are longer than the three Cu–N (bdmpp) bonds (Table 1), suggesting that the two MeCN molecules may be easily replaced by other strong donor ligands.

Compounds **2**·1.5H_2O and **3**·2MeOH crystallize in the monoclinic space group $P2_1/n$ and the asymmetric unit of **2** contains one discrete [Cu(bdmpp)$(N_3)_2$] molecule and one and a half of the water solvent molecules, while that of **3** has half of the [Cu(bdmpp)(μ-N_3)(N_3)]$_2$ molecule and one methanol solvent molecule. In the structure of **2**, Cu(1) adopts a distorted square-pyramidal geometry (Figure 2). The basal plane is defined by N(1), N(3), and N(5) from the bdmpp ligand and N(6) from a terminal azide. The apical site is occupied by N(9) of the other terminal azide. The axial Cu(1)–N(9) of 2.186(2) Å is slightly longer than the basal Cu–N bonds (Table 1), but shorter than that found in [Cu_2(terpy)$_2$-μ-$(N_3)_2(N_3)_2Cu_3$-μ-$(N_3)_4(N_3)_2$] [terpy = 2,2′:6′,2′′-terpyridine, 2.288(3) Å].[20] It is noted that Cu(1) displaces 0.3613 Å out of the N(1)–N(3)–N(5)–N(6) least-squares plane, which causes the *trans* angles in the basal plane to deviate significantly from 180°.

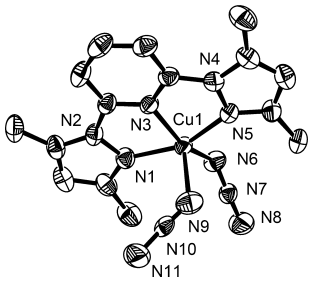

Figure 2. Molecular structure of **2** with 50% thermal ellipsoids. All hydrogen atoms are omitted for clarity.

As shown in Figure 3, **3** consists of two [Cu(bdmpp)-(N_3)]$^+$ fragments that are bridged by a pair of end-on bridging N_3^- anions, forming a centrosymmetric dimetallocyclic Cu_2N_2 core structure. The Cu_2N_2 core is symmetric and the Cu(1)···Cu(1A) contact is 3.263(13) Å, which excludes any metal–metal interaction. Each Cu atom adopts a distorted octahedral geometry, where N(1), N(3), and N(5) of the bdmpp ligand and N(6) of the bridge azide occupy the equatorial sites, and N(6A) and N(9) from one bridging and one terminal azide sit at the two apical sites. The Cu atom lies 0.1024 Å out of the equatorial plane. The average Cu–N_{apical} bond [2.128(4) Å] is slightly longer than the average Cu–$N_{equatorial}$ bond [2.075(4) Å] (Table 1).

Compound **4** crystallizes in the triclinic space group $P\bar{1}$ and the asymmetric unit contains half of the [{Cu(bdmpp)(ClO_4)}$_2$(μ-4,4′-bipy)]$^{2+}$ dication and one ClO_4^- anion. The centrosymmetric structure of the dication contains two [Cu(bdmpp)(ClO_4)]$^+$ fragments bridged by one 4,4′-bipy ligand (Figure 4). As indicated in Table 2, Cu(1) in each [Cu(bdmpp)(ClO_4)]$^+$ fragment takes a distorted square-pyramidal geometry, coordinated by N(1), N(3), and N(5) from the bdmpp ligand and N(6) from 4,4′-bipy, which are in equatorial positions, and O(1) from one

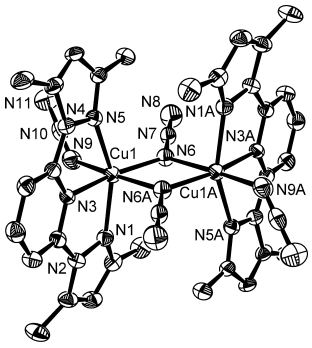

Figure 3. Molecular structure of **3** with 50% thermal ellipsoids. All hydrogen atoms are omitted for clarity.

ClO_4^-, which occupies the apical site. Cu(1) sits over the basal plane with out-of-plane displacement of 0.1688 Å. The Cu(1)–N bond lengths are similar to those of **2**, while the Cu(1)–O bond length [2.2856(18) Å] is comparable to that observed in complexes containing square-pyramidally coordinated Cu^{II} [Cu(pr2pz)$(ClO_4)_2$] [pr2pz = 1,2-bis[5-methyl-3-(2-methylpropyl)amino-1*H*-pyrazol-1-yl]ethane, 2.451(3) Å].[32]

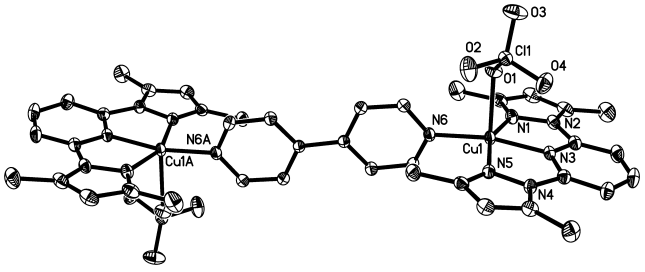

Figure 4. Perspective view of the [{Cu(bdmpp)(ClO_4)}$_2$(μ-4,4′-bipy)]$^{2+}$ dication of **4** with 50% thermal ellipsoids. All hydrogen atoms are omitted for clarity.

Compound **5** crystallizes in the monoclinic space group $C2/c$ and the asymmetric unit consists of one [Cu(bdmpp)(μ-dca)]$^+$ cation and one ClO_4^- anion. Like that of the Cu center of **1**, Cu(1) in the cation of **5** adopts a distorted trigonal-bipyramidal geometry, coordinated by N(3) of the bdmpp ligand and N(6) and N(8A) atoms of μ-dca (in equatorial positions), and N(1) and N(5) of the bdmpp ligand (in apical positions) (Figure 5). The bond lengths and angles around Cu(1) in **5** (Table 2) are similar to those observed in **1**. Topologically, the [Cu(bdmpp)]$^{2+}$ fragment in **5** works as a two-connecting node, which is linked to two equivalent nodes through Cu-μ-dca-Cu bridges to form a 1D [Cu(bdmpp)(μ-dca)]$_n^{n+}$ chain extending along the *b* axis. It is worth noting that the bdmpp ligands covering the chain are parallel to each other and have the same direction. Two neighboring bdmpp ligands linked by one dca may be visualized as a molecular clip with a diameter of 7.4952(3) Å [Cu(1)···Cu(1A) contact]. Thus, the structure of **5** may be best described as a unique 1D chain of clips, each of which "clamps" one ClO_4^- anion inside it.

Table 2. Selected bond lengths [Å] and angles [°] of **4**–**6**.[a]

		Compound **4**	
Cu(1)–N(1)	2.004(2)	Cu(1)–N(6)	1.975(2)
Cu(1)–N(3)	1.944(2)	Cu(1)–O(1)	2.2856(18)
Cu(1)–N(5)	2.026(2)		
N(1)–Cu(1)–N(3)	79.55(9)	N(5)–Cu(1)–N(6)	99.35(8)
N(3)–Cu(1)–N(5)	79.10(8)	N(1)–Cu(1)–O(1)	89.49(8)
N(5)–Cu(1)–N(1)	158.06(8)	N(3)–Cu(1)–O(1)	98.36(7)
N(1)–Cu(1)–N(6)	100.44(8)	N(5)–Cu(1)–O(1)	98.55(7)
N(3)–Cu(1)–N(6)	167.73(8)	N(6)–Cu(1)–O(1)	93.90(8)
		Compound **5**	
Cu(1)–N(1)	1.991(3)	Cu(1)–N(6)	2.059(3)
Cu(1)–N(3)	1.974(3)	Cu(1)–N(8A)	2.075(3)
Cu(1)–N(5)	2.008(3)		
N(1)–Cu(1)–N(3)	78.56(11)	N(5)–Cu(1)–N(8A)	94.84(12)
N(3)–Cu(1)–N(5)	78.09(11)	N(1)–Cu(1)–N(6)	95.80(11)
N(5)–Cu(1)–N(1)	156.63(11)	N(3)–Cu(1)–N(6)	131.78(11)
N(1)–Cu(1)–N(8A)	100.51(12)	N(5)–Cu(1)–N(6)	98.94(12)
N(3)–Cu(1)–N(8A)	128.69(11)	N(6)–Cu(1)–N(8A)	99.51(12)
		Compound **6**	
Cu(1)–N(1)	1.995(2)	Cu(1)–N(8A)	2.448(3)
Cu(1)–N(3)	1.949(2)	Cu(1)–N(6)	1.932(2)
Cu(1)–N(5)	2.013(2)		
N(3)–Cu(1)–N(5)	79.33(8)	N(5)–Cu(1)–N(6)	100.51(9)
N(1)–Cu(1)–N(3)	79.30(8)	N(1)–Cu(1)–N(8A)	88.02(9)
N(5)–Cu(1)–N(1)	158.46(8)	N(3)–Cu(1)–N(8A)	90.49(10)
N(1)–Cu(1)–N(6)	99.76(9)	N(5)–Cu(1)–N(8A)	94.82(9)
N(3)–Cu(1)–N(6)	167.43(8)	N(6)–Cu(1)–N(8A)	102.3(10)

[a] Symmetry codes for **5**: A: x, $y - 1$, z; for **6**: A: $-x + 1/2$, $y - 1/2$, $-z + 1/2$.

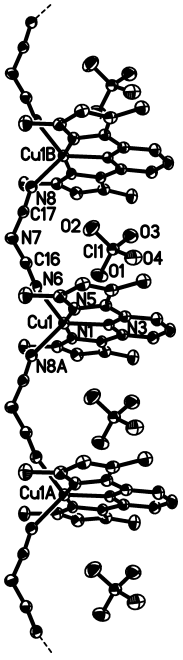

Figure 5. View of a section of the chain of **5** (extending along the *b* axis) with 50% thermal ellipsoids. All hydrogen atoms are omitted for clarity.

Compound **6** crystallizes in the monoclinic space group $P2_1/n$, and the asymmetric unit consists of one $[Cu(bdmpp)(\mu\text{-}N_3)]^+$ cation, one ClO_4^- anion, and one MeCN solvent molecule. The $[Cu(bdmpp)]^{2+}$ fragment of **6** again acts as a two-connecting node, which is connected to the equivalent nodes through end-to-end bridging N_3^- to form a 1D spiral chain extending along the *b* axis (Figure 6). The average chain-to-chain separation is 3.9 Å, and there are no evident interactions between the cationic chains and the counteranions and MeCN solvent molecules. For the $[Cu(bdmpp)(\mu\text{-}N_3)]^+$ cation of **6**, the Cu(1) atom adopts a similar coordination geometry to that of **2**, coordinated by N(1), N(3), and N(5) of the bdmpp ligand, and N(6) of one azide anion (in equatorial sites) and N(8A) of the other azide anion (in apical site). As listed in Table 2, one end-to-end bridging Cu(1)–N(8A) bond [2.448(2) Å] is 0.5 Å longer than the other one [Cu(1)–N(6)], which may be due to the requirement for the formation of the spiral chain. Other bond lengths and angles around Cu(1) in **6** are comparable to those of the corresponding ones of **2**.

Compound **7** crystallizes in the triclinic space group $P\bar{1}$ and the asymmetric unit contains half of the $[\{Cu(bdmpp)(N_3)\}_2(\mu\text{-}N_3)_2Cu(N_3)_2]$ molecule. The molecular structure of **7** is shown in Figure 7 and the selected bond lengths and angles are listed in Table 3. In this structure, the framework of **2** is almost retained. Two molecules of **2** link a $Cu(N_3)_2$ species through two end-on bridging azide anions to form a sandwich structure. Alternatively, the structure may be viewed as a centrosymmetric sandwich structure, in which one planar $[Cu(N_3)_2(\mu\text{-}N_3)_2]^{2-}$ anion is placed in between two planar $[Cu(bdmpp)(N_3)]^+$ cations through a pair of Cu-μ-N_3-Cu bridges. The skeleton planes of the two bdmpp ligands are almost parallel but with opposite orientations, and their separation is about 6.3 Å. In

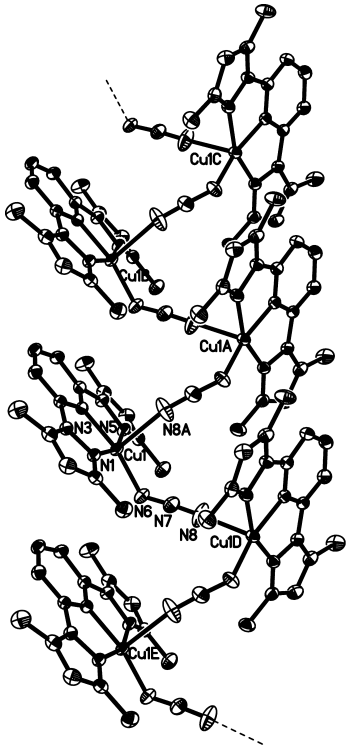

Figure 6. View of a section of the chain of **6** (extending along the *b* axis) with 50% thermal ellipsoids. All hydrogen atoms are omitted for clarity.

the $[Cu(bdmpp)(N_3)]^+$ cations, Cu(1) or Cu(1A) has a square-pyramidal geometry. The Cu(1)–N (bdmpp) and Cu(1)–N (terminal N_3^-) bond lengths are similar to those of **2**. The end-on bridging Cu(1)–N(9) bond is slightly longer than the corresponding bond of **2** and shorter than that of **6**. For the $[Cu(N_3)_2(\mu\text{-}N_3)_2]^{2-}$ anion, Cu(2) has a typical square-planar geometry, coordinated by two terminal and two end-on bridging azide anions. The bridging Cu(2)–N(9) bond [2.343(2) Å] is 0.38 Å longer than the terminal Cu(2)–N(12) bond.

Compounds **8** and **9** crystallize in the triclinic space group $P\bar{1}$ and the asymmetric unit contains half of the $[Cu(\mu\text{-}N_3)(bdmpp)(\mu\text{-}N_3)M(\mu\text{-}N_3)(X)]_2$ molecule (**8**: M = Co, X = N_3; **9**: M = Ni, X = Cl) and two MeCN solvent molecules for **9**. Compounds **8** and **9** have a 1D chain structure (extending along the *c* axis) in which $[Cu(\mu\text{-}N_3)(bdmpp)(\mu\text{-}N_3)M(\mu\text{-}N_3)(X)]_2$ molecules are linked by

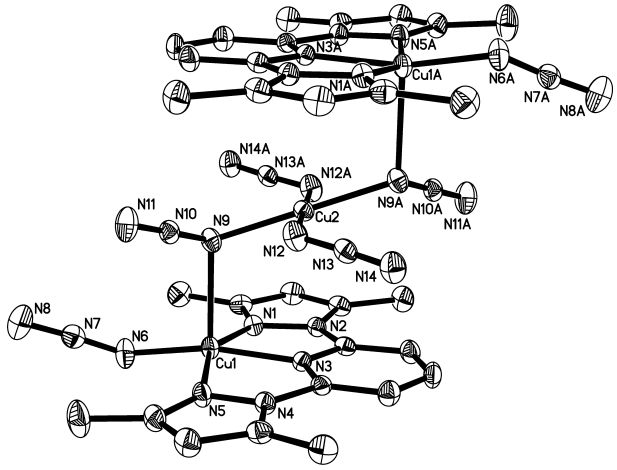

Figure 7. Perspective view of **7** with 50% thermal ellipsoids. All hydrogen atoms are omitted for clarity.

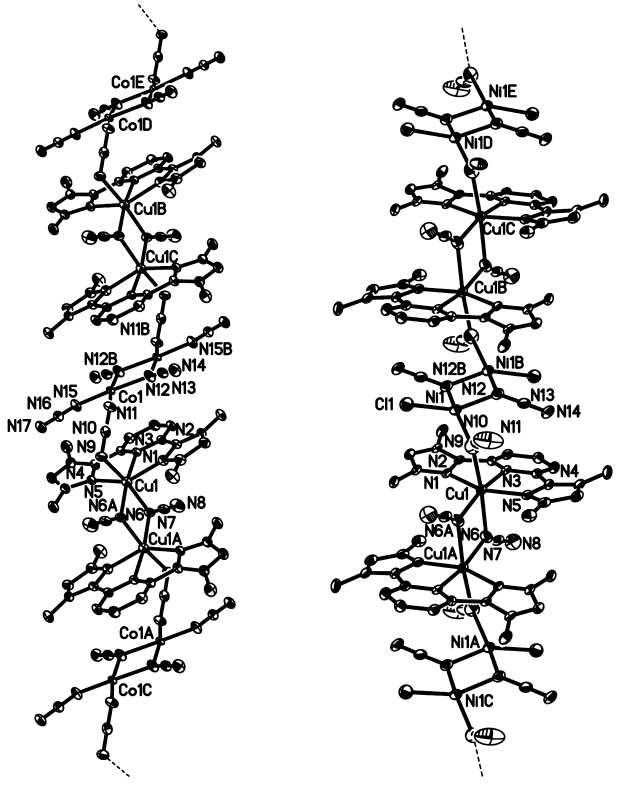

Figure 8. View of a section of the chain of **8** (left) and **9** (right) (extending along the *c* axis) with 50% thermal ellipsoids. All hydrogen atoms are omitted for clarity.

Table 3. Selected bond length [Å] and angles [°] of **7**.[a]

Cu(1)–N(6)	1.918(2)	Cu(1)–N(9)	2.343(2)
Cu(1)–N(3)	1.964(2)	Cu(1)–N(1)	2.046(2)
Cu(1)–N(5)	2.045(2)	Cu(2)–N(12)	1.961(2)
Cu(2)–N(9)	2.003(2)		
N(6)–Cu(1)–N(5)	102.27(10)	N(6)–Cu(1)–N(9)	100.88(10)
N(6)–Cu(1)–N(3)	166.43(10)	N(3)–Cu(1)–N(9)	92.50(9)
N(3)–Cu(1)–N(5)	78.45(9)	N(5)–Cu(1)–N(9)	95.66(9)
N(6)–Cu(1)–N(1)	98.50(10)	N(1)–Cu(1)–N(9)	94.75(9)
N(3)–Cu(1)–N(1)	77.92(9)	N(12)–Cu(2)–N(9A)	90.91(10)
N(5)–Cu(1)–N(1)	154.52(9)	N(12)–Cu(2)–N(9)	89.09(10)

[a] Symmetry code: A: $-x + 1, -y, -z + 1$.

end-to-end azide anions (**8**) (Figure 8, left) or end-on azide anions (**9**) (Figure 8, right). Each $[Cu(\mu\text{-}N_3)(bdmpp)(\mu\text{-}N_3)\text{-}M(\mu\text{-}N_3)(X)]_2$ molecule consists of one centrosymmetric $[Cu(bdmpp)(\mu\text{-}N_3)]_2^{2+}$ dication and one centrosymmetric $[(\mu\text{-}N_3)M(\mu\text{-}N_3)(X)]_2^{2-}$ dianion linked by one end-to-end azide (**8**) or one end-on azide (**9**). The structure of the dication in **3** is almost kept in the structures of **8** and **9**. Each Cu atom in **8** or **9** adopts a distorted octahedral geometry, coordinated by three N atoms from one bdmpp ligand and three N atoms from one end-to-end and two end-on azides (**8**) or three end-on azides (**9**). In this case, the end-to-end bridging Cu(1)–N(9) bond of **8** is even shorter than the end-on bridging Cu(1)–N(9) in **9** (Table 4). Other bond lengths and angles around Cu in **8** or **9** are similar to those of the corresponding ones of **3**. The Cu(1)···Cu(1A) separation is 3.2105(14) Å for **8** and 3.3779(13) Å for **9**.

Within the dianion of **8**, each Co atom is coordinated by one terminal, one end-to-end bridging, and two bridging azides, forming a square-planar geometry. The Co(1)···Co(1B) contact is 3.1234(13) Å while the Cu(1)···Co(1) contact between the dication and dianion is 4.4064(13) Å. The mean Co(1)–N bond length [1.966(4) Å] is similar to that found in $[PPh_4][Co(N_3)_3Cl]$[33] [Co–N 1.946(3) Å]. However, in the structure of the anion of **9**, each Ni atom also adopts a square-planar geometry, coordinated by one terminal Cl atom and three end-on bridging azides. The Ni(1)···Ni(1B) contact is 3.091(2) Å while the Cu(1)···Ni(1) contact between the dication and dianion is 3.5670(12) Å. The terminal Ni(1)–Cl(1) bond [2.2499(19) Å] is longer than that found in [(L)NiKCl·3THF] [L = *N*,*N*′-bis(2,6-diisopropylphenyl)-2,6-pyridinedicarboxamido, 2.1688(17) Å],[34] while the Ni–N bond is slightly longer than that in $[L^1Ni(N_3)]$ [L^1 = $Me_2NCH_2CH_2N(Me)C_6H_4OH$, 1.905(7) Å].[35]

The electrochemical behaviors of **1**–**9** have been investigated by cyclic voltammetry (CV) in DMF containing 0.1 M tetraethylammonium perchlorate (TEAP). The electrochemical data are summarized in Table 5. Under similar experimental conditions, the electrochemical studies of the free ligand using the cyclic voltammetry showed no electrochemical activity within the scanned potential window. Thus, the electrochemical waves observed in the cyclic voltammograms of **1**–**9** are only metal-based.

All the complexes show the quasireversible redox process with a potential of about 0.00 V in the cathode and about

Table 4. Selected bond lengths [Å] and angles [°] of **8** and **9**.[a]

	Compound **8**		
Cu(1)–N(6A)	2.030(4)	Cu(1)–N(9)	2.235(4)
Cu(1)–N(5)	2.089(4)	Co(1)–N(15)	1.919(4)
Cu(1)–N(3)	2.094(4)	Co(1)–N(11)	1.958(5)
Cu(1)–N(1)	2.104(4)	Co(1)–N(12)	1.990(4)
Cu(1)–N(6)	2.140(4)	Co(1)–N(12B)	1.997(5)
N(3)–Cu(1)–N(6A)	168.11(16)	N(6)–Cu(1)–N(6A)	79.37(18)
N(5)–Cu(1)–N(3)	74.76(16)	N(5)–Cu(1)–N(6)	96.79(17)
N(6)–Cu(1)–N(1A)	108.23(18)	N(6)–Cu(1)–N(9)	167.97(16)
N(5)–Cu(1)–N(1)	146.19(15)	N(15)–Co(1)–N(11)	99.5(2)
N(3)–Cu(1)–N(1)	73.94(16)	N(15)–Co(1)–N(12)	166.9(2)
N(5)–Cu(1)–N(6A)	105.04(17)	N(11)–Co(1)–N(12)	91.59(19)
N(3)–Cu(1)–N(6)	88.83(15)	N(15)–Co(1)–N(12B)	92.21(19)
N(1)–Cu(1)–N(6)	95.05(17)	N(11)–Co(1)–N(12B)	168.31(18)
N(9)–Cu(1)–N(6A)	88.68(16)	N(12)–Co(1)–N(12B)	76.8(2)
N(5)–Cu(1)–N(9)	87.56(17)	Cu(1)–N(6)–Cu(1B)	100.63(18)
N(3)–Cu(1)–N(9)	103.15(15)	Co(1)–N(12)–Co(1B)	103.2(2)
N(1)–Cu(1)–N(9)	87.35(17)		
	Compound **9**		
Cu(1)–N(3)	1.999(4)	Cu(1)–N(9)	2.253(7)
Cu(1)–N(6A)	2.010(5)	Ni(1)–N(9)	1.963(5)
Cu(1)–N(5)	2.061(4)	Ni(1)–N(12B)	1.976(4)
Cu(1)–N(1)	2.089(4)	Ni(1)–N(12)	1.986(4)
Cu(1)–N(6)	2.345(7)	Ni(1)–Cl(1)	2.2499(19)
N(3)–Cu(1)–N(5)	78.26(15)	N(5)–Cu(1)–N(6)	89.97(16)
N(5)–Cu(1)–N(6A)	101.12(17)	N(1)–Cu(1)–N(6)	92.60(16)
N(3)–Cu(1)–N(1)	77.35(14)	N(9)–Cu(1)–N(6)	173.88(18)
N(1)–Cu(1)–N(6A)	103.48(17)	N(9)–Ni(1)–N(12B)	154.3(2)
N(3)–Cu(1)–N(6A)	165.3(2)	N(9)–Ni(1)–N(12)	94.3(2)
N(5)–Cu(1)–N(1)	155.29(14)	N(12)–Ni(1)–N(12B)	77.5(2)
N(3)–Cu(1)–N(9)	99.16(17)	N(9)–Ni(1)–Cl(1)	101.29(19)
N(9)–Cu(1)–N(6A)	95.5(3)	Cl(1)–Ni(1)–N(12B)	96.34(14)
N(5)–Cu(1)–N(9)	92.56(18)	N(12)–Ni(1)–Cl(1)	152.95(14)
N(1)–Cu(1)–N(9)	87.43(17)	Ni(1)–N(9)–Cu(1)	115.4(3)
N(3)–Cu(1)–N(6)	86.81(17)	Ni(1)–N(12)–Ni(1B)	102.5(2)
N(6)–Cu(1)–N(6A)	78.5(3)	Cu(1)–N(6)–Cu(1)	101.5(3)

[a] Symmetry codes for **8**: A: $-x + 1, -y, -z$; B: $-x + 1, -y, -z + 1$; for **9**: A: $-x + 1, -y + 2, -z + 1$; B: $-x + 1, -y + 2, -z$.

Table 5. Electrochemical data of complexes **1**–**9**.[a]

Complexes	**1**	**2**	**3**	**4**	**5**	**6**	**7**	**8**	**9**
E_I [V]	–0.01	–0.06	–0.05	0.02	0.09	0.02	0.01	–0.09	–0.02
E_I' [V]	0.18	0.24	0.33	0.21	0.24	0.22	0.56	0.22	0.59
$E_{1/2}$ [V]	0.09	0.15	0.19	0.09	0.07	0.10	0.12	0.15	0.30
ΔE_I [V]	0.19	0.30	0.38	0.19	0.15	0.20	0.55	0.31	0.61
E_{II} [V]	–0.42	–0.59	–0.57	–0.48	–0.42	–0.54	–0.63	–0.52	–0.66
E_{II}' [V]	0.04	–	–	0.06	–0.03	–	–0.20	–0.18	–0.18
$E_{1/2}$ [V]	–0.23	–	–	–0.23	–0.19	–	–0.42	–0.35	–0.47
ΔE_{II} [V]	0.46	–	–	0.57	0.39	–	–0.43	0.34	0.48
E_{III} [V]			–	–	–	–	–1.26	–1.28	–1.03
E_{III}' [V]	–	–	–	–	–	–	0.13	0.02	–0.12

[a] Measured by CV at scan rate of 0.1 V/s; 1.0 mM in DMF containing 0.1 M TEAP for all complexes with a concentration of 1×10^{-3} M. Condition: working electrode, Pt plate (2×2 mm^2); counter electrode, Pt wire; reference electrode, SCE.

0.22 V in the anode (except 0.33 V for **3**, 0.56 V for **7**, and 0.59 V for **9**) (Figure 9), corresponding to the change from Cu^{II} species to Cu^{I} species. When the CV measurements were performed at different scan rates such as 0.05, 0.1, 0.2, and 0.5 V/s, it was found that the ratio of cathodic to anodic peak current was close to unity, especially for a lower scan rate, suggesting this first step is a quasireversible reduction process.[36] The second reduction waves in the range of –0.40 to –0.70 V for **1**, **4**, **5**, **7**, **8**, and **9** are quasireversible and due to the formation of Cu^{I} species followed by the deposition of Cu^0 onto the electrode surface as judged by the appearance on the reverse scan of a greater anodic peak current at the corresponding potential E_{II}' than that of the cathode.[37] The separation between the potentials of the first redox couple for all complexes is ΔE_I = 0.15 V or greater and the weak peak current at E_{II} indicates that a geometrical reorganization, hindered to a large extent by the low flexibility of the coordination sphere, is involved in the reduction process.[36] After several cycles, the color of solutions of these complexes became light and more metal particles were found on the electrode surface. These facts were the evidence of the decomposition of the complexes during the CV measurement.

Compared to the second reduction wave of their precursor **1**, those of **4** and **6** are very weak and the potential shift negative (Figure 9a), while the second reduction electrochemical response and potential of **5** are almost the same as **1**. These facts indicate that the stronger binding of azide and 4,4′-bipy ligands to the metal center and the coordination sphere is more stable than that of dca and acetonitrile ligands.

The large difference of ΔE_I value (0.55 V for **7** and 0.61 V for **9**) between the the potentials of the first redox couple is consistent with the stronger spin–spin interaction of metals. Further reductions at E_{III} = –1.26 V for **7**, –1.28 V for **8**, and –1.03 V for **9** are almost totally irreversible, which may be due to the deposition of Cu^0 (planar Cu), Co^0, and Ni^0 onto the electrode surface as judged by the appearance of a sharp anodic peak at E_{III}' = 0.18, 0.02, and –0.12 V for **7**, **8**, and **9**, corresponding to the redissolution of Cu^0, Co^0, and Ni^0, respectively.

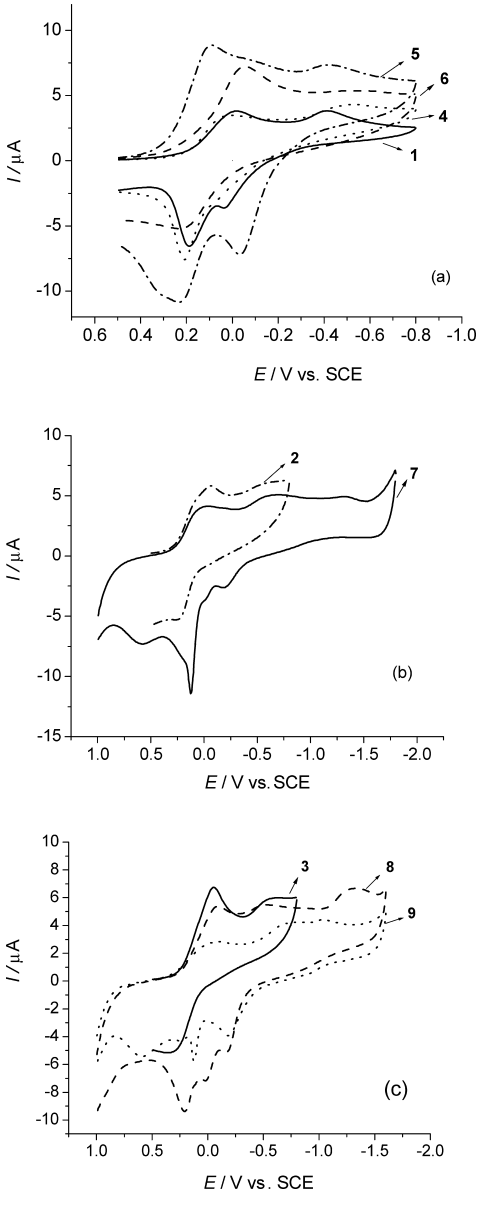

Figure 9. Cyclic voltammograms of complexes **1**–**9**.

Conclusions

In this paper, we demonstrated our new approaches to the assembly of a set of homometallic or heterometallic coordination oligomers and polymers from reactions of preformed complexes **1**–**3** with different linkers 4,4′-bipy, dca, and azide as well as M^{2+} (M = Cu, Co, Ni). In the structures of **4**–**6**, the $[Cu(bdmpp)]^{2+}$ fragment of **1** was retained, even though the copper coordination geometry was changed during the reactions. Compound **4** forms a 4,4′-bipy-bridged dimer structure, while **5** and **6** show a 1D dca-bridged chain of clips and a 1D spiral azido-bridged chain, respectively. In this structure of **7**, the structure of **2** was kept and two molecules of **2** connect a $Cu(N_3)_2$ species through two end-on bridging azide anions to form a sandwich structure. In the structure of **8** or **9**, the structure of **3** was retained, and the $[Cu(bdmpp)(\mu\text{-}N_3)(\mu\text{-}N_3)]_2$ molecules of **3** interconnect with the $[M(\mu\text{-}N_3)(X)]_2$ molecules through end-to-end azides (**8**) or end-on azides (**9**) to form a 1D chain structure. Electrochemical studies on **1**–**9** revealed that one quasireversible redox wave was observed at higher potential for all these complexes, while, **1**, **4**, **5**, **7**, **8**, and **9** showed the second quasireversible redox wave at lower potentials. It is concluded that though the assembled products retain the $[Cu(bdmpp)]^{2+}$ fragment of **1** or the whole molecule **2** or **3**, their electrochemical properties are influenced by the bridging ligands around the Cu center of the fragment or other metal ions introduced in their frameworks. The interesting topological structures of **4**–**9** make **1**–**3** very promising precursors for the synthesis of homo- and heterometallic coordination oligomers and polymers. We are currently extending this work by studies on the synthesis of novel homo- or heterometallic coordination oligomers and polymers from reactions of **1**–**3** with other polydentate donor ligands such as 5,10,15,20-tetra(4-pyridyl)-21*H*,23*H*-porphyrin and 2,4,6-tri(4-pyridyl)-1,3,5-triazine, and other main group metals (Pb^{2+}, Bi^{3+}) and transition metals (Zn^{2+}, Cd^{2+}, Hg^{2+}, etc.).

Experimental Section

General Remarks: Compounds bdmpp[38] and $[Cu(MeCN)_4](ClO_4)_2$[39] were prepared according to the literature method. All other reagents were used as purchased. The IR spectra were recorded with a Varian 1000 FTIR spectrometer as KBr disk (4000–400 cm^{-1}). The elemental analyses for C, H, and N were performed on an EA1110 CHNS elemental analyzer. Cyclic voltammetry was carried out at 0.1 V/s under oxygen-free conditions using a three-electrode cell with platinum film electrode as working electrode, platinum wire as counter electrode, and SCE as reference electrode. In DMF solution, tetraethylammonium perchlorate (TEAP) was used as the supporting electrolyte.

$[Cu(bdmpp)(MeCN)_2](ClO_4)_2$ (1): bdmpp (0.027 g, 0.1 mmol) was added to a blue solution containing $[Cu(MeCN)_4](ClO_4)_2$ (0.043 g, 0.1 mmol) in MeCN (10 mL). The resulting green solution was stirred for about 0.5 h and then filtered. Diethyl ether (20 mL) was layered onto the filtrate to form green blocks of **1** (0.052 g, 85% based on bdmpp) in several days. IR (KBr disc): $\tilde{\nu}$ = 3137 (m), 2249 (m), 1614 (s), 1566 (s), 1486 (s), 1392 (s), 1320 (s), 1295 (s), 1144 (s), 1106 (s), 1059 (s), 995 (s), 795 (m), 743 (m), 622 (s) cm^{-1}. $C_{19}H_{23}Cl_2CuN_7O_8$ (611.88): calcd. C 37.30, H 3.79, N 16.02; found C 37.46, H 3.56, N 15.90.

$[Cu(bdmpp)(N_3)_2]\cdot 1.5H_2O$ ($2\cdot 1.5H_2O$): NaN_3 (0.013 g, 0.2 mmol) was added to a blue solution containing $CuCl_2\cdot 2H_2O$ (0.017 g, 0.1 mmol) in MeOH (5 mL) and H_2O (5 mL). The solution turned deep brown instantly and bdmpp (0.027 g, 0.1 mmol) was added. The resulting deep green solution was stirred for about 0.5 h and then filtered. Slow evaporation of solvents from the solution for 2 weeks produced deep green crystals of $\mathbf{2}\cdot 1.5H_2O$ (0.033 g, 75% based on bdmpp). IR (KBr disc): $\tilde{\nu}$ = 3144 (w), 2924 (w), 2068 (vs), 2040 (vs), 1614 (vs), 1562 (s), 1488 (vs), 1418 (s), 1392 (s), 1319 (s), 1139 (m), 1054 (m), 986 (m), 799 (m), 740 (m), 675 (w) cm^{-1}. $C_{15}H_{20}CuN_{11}O_{1.5}$ (441.94): calcd. C 40.77, H 4.56, N 34.86; found C 40.46, H 4.42, N 34.91.

$[Cu(bdmpp)(N_3)(\mu\text{-}N_3)]_2\cdot 2MeOH$ ($3\cdot 2MeOH$): Compound $\mathbf{3}\cdot 2MeOH$ (0.032 g, 72% based on bdmpp) was isolated as deep green crystals from the reaction of $CuCl_2\cdot 2H_2O$ (0.017 g, 0.1 mmol), NaN_3 (0.026 g, 0.4 mmol), and bdmpp (0.027 g, 0.1 mmol) in $MeOH/H_2O$ followed by a similar workup to that used in the isolation of **2**. IR (KBr disc): $\tilde{\nu}$ = 3129 (w), 2073 (vs), 2045 (vs), 1614 (s), 1564 (m), 1487 (s), 1389 (m), 1318 (m), 1294 (m), 1141 (w), 1084 (w), 1054 (m), 848 (m), 791 (w), 742 (w), 558 (w) cm^{-1}. $C_{32}H_{42}Cu_2N_{22}O_2$ (893.98): calcd. C 43.00, H 4.74, N 34.47; found C 43.16, H 4.52, N 34.52.

$[\{Cu(bdmpp)(ClO_4)\}_2(\mu\text{-}4,4'\text{-bipy})](ClO_4)_2$ (4): 4,4′-bpy (0.016 g, 0.1 mmol) was added to a green solution containing **1** (0.061 g, 0.1 mmol) in MeCN (10 mL). The mixture was stirred for 10 min, the color of the solution then turned blue, and the solution was filtered. Layering Et_2O (15 mL) onto the filtrate afforded blue blocks of **4** (0.038 g, 63% based on **1**). IR (KBr disc): $\tilde{\nu}$ = 3135 (w), 2996 (w), 1617 (s), 1594 (m), 1564 (m), 1486 (s), 1432 (m), 1390 (m), 1322 (m), 1122 (m), 1087 (s), 1060 (s), 992 (m), 790 (w), 744 (w), 624 (m) cm^{-1}. $C_{40}H_{42}Cl_4Cu_2N_{12}O_{16}$ (1215.76): calcd. C 39.51, H 3.48, N 13.82; found C 40.02, H 3.42, N 13.94.

$\{[Cu(bdmpp)(\mu\text{-dca})](ClO_4)\}_n$ (5): Compound **5** (0.037 g, 75% based on **1**) was isolated as green crystals from the reaction of **1** (0.061 g, 0.1 mmol) and Na(dca) (0.009 g, 0.1 mmol) followed by a similar workup to that used in the isolation of $\mathbf{2}\cdot 1.5H_2O$. IR (KBr disc): $\tilde{\nu}$ = 3130 (w), 2964 (m), 2179 (s), 1618 (s), 1566 (m), 1488 (s), 1370 (m), 1320 (m), 1261 (s), 1093 (s), 1024 (s), 800 (s), 744 (w), 624 (m) cm^{-1}. $C_{17}H_{17}ClCuN_8O_4$ (496.38): calcd. C 41.14, H 3.45, N 22.57; found C 41.26, H 3.22, N 22.44.

$\{[Cu(bdmpp)(\mu\text{-}N_3)](ClO_4)\cdot MeCN\}_n$ (6): Compound **6** (0.041 g, 80% based on **1**) was isolated as deep green crystals from the reaction of **1** (0.061 g, 0.1 mmol) and NaN_3 (0.007 g, 0.1 mmol) followed by a similar workup to that used in the isolation of $\mathbf{2}\cdot 1.5H_2O$. IR (KBr disc): $\tilde{\nu}$ = 3107 (w), 2065 (vs), 2054 (s), 1613 (s), 1565 (m), 1482 (s), 1430 (m), 1391 (m), 1316 (m), 1144 (s), 1118 (s), 1084 (s), 991 (m), 793 (w), 743 (w), 625 (m) cm^{-1}. $C_{17}H_{20}ClCuN_9O_4$ (513.41): calcd. C 39.77, H 3.93, N 24.55; found C 39.64, H 3.76, N 24.72.

$[\{Cu(N_3)(bdmpp)\}_2(\mu\text{-}N_3)_2Cu(N_3)_2]$ (7): NaN_3 (0.026 g, 0.4 mmol) and $CuCl_2\cdot 2H_2O$ (0.017 g, 0.1 mmol) were added to a deep green solution containing **2** (0.044 g, 0.1 mmol) in MeCN (10 mL). The solution was stirred for 20 min; it then darkened and was filtered. Diethyl ether (20 mL) was layered onto the filtrate to form dark brown blocks of **7** (0.033 g, 67% based on **2**) in several days. IR (KBr disc): $\tilde{\nu}$ = 3430.6 (m), 3142 (w), 2066 (vs), 2041 (s), 1614 (s), 1562 (m), 1486 (s), 1418 (m), 1392 (m), 1318 (m), 1139 (m), 1084

(m), 1053 (m), 986 (w), 799 (w), 740 (w) cm^{-1}. $C_{30}H_{34}Cu_3N_{28}$ (977.47): calcd. C 37.04, H 3.52, N 40.32; found C 37.16, H 3.36, N 39.96.

[{Cu(μ-N_3)(bdmpp)(μ-N_3)Co(μ-N_3)(N_3)}$_2$]$_n$ (8): Compound **8** (0.056 g, 50% based on **3**) was isolated as dark green crystals from the reaction of **3** (0.089 g, 0.1 mmol), $CoCl_2·6H_2O$ (0.048 g, 0.2 mmol), and NaN_3 (0.052 g, 0.8 mmol) followed by a similar workup to that used in the isolation of **7**. IR (KBr disc): $\tilde{\nu}$ = 3432 (w), 3133 (w), 2963 (m), 2066 (vs), 2029 (s), 1608 (s), 1562 (m), 1473 (s), 1388 (m), 1372 (m), 1293 (m), 1261 (s), 1096 (m), 1031 (m), 986 (w), 793 (s), 741 (w) cm^{-1}. $C_{30}H_{34}Co_2Cu_2N_{34}$ (1115.85): calcd. C 32.29, H 3.07, N 42.68; found C 32.12, H 3.32, N 42.24.

[{Cu(μ-N_3)(bdmpp)(μ-N_3)Ni(μ-N_3)Cl}$_2$·4MeCN]$_n$ (9): Compound **9** (0.062 g, 49% based on **3**) was isolated as dark green crystals from

Table 6. Crystallographic data for **1**, **2**·1.5H_2O, **3**·2MeOH, **4**, and **5**.

Compounds	**1**	**2**·1.5H_2O	**3**·2MeOH	**4**	**5**
Formula	$C_{19}H_{23}Cl_2CuN_7O_8$	$C_{15}H_{20}Cu_1N_{11}O_{1.5}$	$C_{32}H_{42}Cu_2N_{22}O_2$	$C_{40}H_{42}Cl_4Cu_2N_{12}O_{16}$	$C_{17}H_{17}ClCuN_8O_4$
M_r	611.88	441.94	893.98	1215.76	496.38
Temperature [K]	193(2)	153(2)	153(2)	153(3)	153(3)
Crystal system	orthorhombic	monoclinic	monoclinic	triclinic	monoclinic
Space group	*Pbca*	$P2_1/n$	$P2_1/n$	$P\bar{1}$	$C2/c$
a [Å]	12.626(3)	11.201(2)	8.9002(18)	7.6768(15)	24.4394(9)
b [Å]	14.821(3)	11.629(2)	12.487(3)	8.9909(18)	7.4925(3)
c [Å]	27.060(5)	14.927(3)	17.473(4)	17.265(3)	21.4748(8)
α [°]				99.49(3)	
β [°]		103.89(3)	99.65(3)	91.54(3)	95.100(10)
γ [°]				91.46(3)	
V [Å^3]	5063.6(18)	1887.4(6)	1914.5	1174.4(4)	3912.8(3)
Z	8	2	2	1	8
D_{calcd} [g/cm^3]	1.605	1.552	1.551	1.719	1.685
F(000)	2504	908	924	620	2024
μ [mm^{-1}]	1.132	1.193	1.175	1.219	1.298
Total reflections	45277	18050	18303	11618	17961
Unique reflections	4618 (R_{int} = 0.0460)	4313 (R_{int} = 0.0328)	3494 (R_{int} = 0.0756)	5351 (R_{int} = 0.0184)	4469 (R_{int} = 0.0457)
Obsd. reflections	4492	3870	2876	4970	3770
Parameters	340	285	271	364	285
R_1[a]	0.0445	0.0346	0.0682	0.0347	0.0614
wR_2[b]	0.1208	0.0998	0.1379	0.1129	0.1713
S[c]	1.015	1.064	1.088	1.074	1.072
Residual peaks [e/Å^3]	0.490, –0.416	0.523, –0.522	0.573, –0.452	0.697, –0.831	1.283, –2.402

[a] $R_1 = \Sigma||F_o| - |F_c||/\Sigma|F_o|$. [b] $wR_2 = \{w\Sigma(|F_o| - |F_c|)^2/\Sigma w|F_o|^2\}^{1/2}$. [c] $S = \{\Sigma w(|F_o| - |F_c|)^2/(n - p)\}^{1/2}$, where *n* is the number of reflections and *p* is the total number of parameters refined.

Table 7. Crystallographic data for **6**–**9**.

Compounds	**6**	**7**	**8**	**9**
Formula	$C_{17}H_{20}ClCuN_9O_4$	$C_{30}H_{34}Cu_3N_{28}$	$C_{30}H_{34}Co_2Cu_2N_{34}$	$C_{38}H_{46}Cl_2Cu_2N_{32}Ni_2$
M_r	513.41	977.47	1115.85	1266.47
Temperature [K]	193(2)	193(2)	153(2)	153(2)
Crystal system	monoclinic	triclinic	triclinic	triclinic
Space group	$P2_1/n$	$P\bar{1}$	$P\bar{1}$	$P\bar{1}$
a [Å]	12.821(3)	8.6789(17)	9.3824(19)	11.852(2)
b [Å]	7.2431(14)	10.594(2)	9.4618(19)	11.868(2)
c [Å]	23.237(5)	10.760(2)	13.615(3)	11.910(2)
α [°]		90.38(3)	106.55(3)	102.21(3)
β [°]	98.38(3)	102.31(3)	97.90(3)	112.52(3)
γ [°]		95.51(3)	104.33(3)	112.14(3)
V [Å^3]	2134.9(7)	961.7(3)	1094.0(4)	1303.5(5)
Z	4	1	1	1
D_{calcd} [g/cm^3]	1.597	1.688	1.694	1.613
F(000)	1052	497	564	646
μ [mm^{-1}]	1.194	1.711	1.774	1.684
Total reflections	19889	9259	10626	12272
Unique reflections	3901 (R_{int} = 0.0740)	3485(R_{int} = 0.0285)	4944 (R_{int} = 0.0644)	5838 (R_{int} = 0.0628)
Obsd. reflections	3700	3017	3779	4060
Parameters	294	281	311	349
R_1[a]	0.0360	0.0348	0.0600	0.0636
wR_2[b]	0.0922	0.0831	0.1817	0.1711
S[c]	1.062	1.084	1.009	1.082
Residual peaks [e/Å^3]	0.459, –0.429	0.340, –0.428	1.463, –2.114	1.404, –1.343

[a] $R_1 = \Sigma||F_o| - |F_c||/\Sigma|F_o|$. [b] $wR_2 = \{w\Sigma(|F_o| - |F_c|)^2/\Sigma w|F_o|^2\}^{1/2}$. [c] $S = \{\Sigma w(|F_o| - |F_c|)^2/(n - p)\}^{1/2}$, where *n* is the number of reflections and *p* is the total number of parameters refined.

the reaction of **3** (0.089 g, 0.1 mmol), $NiCl_2·6H_2O$ (0.048 g, 0.2 mmol), and NaN_3 (0.052, 0.8 mmol) followed by a similar workup to that used in the isolation of **7**. IR (KBr disc): $\tilde{\nu}$ = 3433 (m), 3129 (w), 2963 (m), 2085 (s), 2069 (vs), 1613 (s), 1566 (m), 1485 (s), 1420 (m), 1392 (m), 1318 (m), 1261 (s), 1179 (m), 1095 (m), 1024 (s), 988 (m), 801 (s), 740 (w), 670 (w) cm^{-1}. $C_{38}H_{46}Cl_2Cu_2N_{32}Ni_2$ (1266.47): calcd. C 36.04, H 3.66, N 35.39; found C 35.82, H 3.52, N 35.33.

X-ray Structure Determinations: X-ray-quality crystals of **1**, **2**·1.5H_2O, **3**·2MeOH, and **4**–**9** were obtained directly from the above preparations. Measurements of **1**, **3**·2MeOH, **6**, and **7** were made on a Rigaku Mercury CCD X-ray diffractometer by using graphite-monochromated Mo-K_α (λ = 0.71070 Å). Single crystals were mounted with grease at the top of a glass fiber and cooled to 193 K in a liquid N_2 stream. Cell parameters were refined using the program CrystalClear (Rigaku and MSC, version 1.3, 2001). The collected data were reduced using the program CrystalClear (Rigaku and MSC, version 1.3, 2001) while an absorption correction (multiscan) was applied. Measurements of **2**·1.5H_2O, **4**, **5**, **8**, and **9** were made on a Rigaku *R*-axis Spider diffractometer with graphite-monochromated Mo-K_α radiation (λ = 0.71073 Å) at 153 K. Data reductions and absorption corrections were performed with the SAINT and SADABS software packages.

All the structures were solved by direct methods and refined on F^2 by full-matrix least-squares methods with the SHELXTL-97 program.[40] In the case of **2**·1.5H_2O, one water solvent molecule was found to be disordered over two orientations with an occupancy ratio of O(1)/O(1′) = 0.533/0.467. the other water solvent molecule was modeled with an occupancy factor of 0.5. For **4**, one ClO_4^- anion was found to be split over two orientations by rotation around the Cl(2)–O(5) bond, which were refined with occupancy factors of 0.455:0.545 for O(6)/O(6′), O(7)/O(7′), and O(8)/O(8′). All non-hydrogen atoms were refined anisotropically. The H atoms of the water solvent molecules in **2**·1.5H_2O and that of the hydroxy group of the methanol solvent molecule in **3** were located from the Fourier maps. All other H atoms on C atoms were placed in geometrically idealized positions C–H 0.98 Å for methyl groups; C–H 0.95 Å for phenyl groups and pyrazole ring; and constrained to ride on their parent atoms with U_{iso}(H) = 1.2U_{eq}(C) for phenyl groups and pyrazole ring and U_{iso}(H) = 1.5U_{eq}(C) for methyl groups. A summary of the key crystallographic information for **1**, **2**·1.5H_2O, **3**·2MeOH, and **4**–**9** is given in Tables 6 and 7.

CCDC-651925 (for **1**), -651926 (for **2**·1.5H_2O), -651927 (for **3**·2MeOH), -651928 (for **4**), -651929 (for **5**), -651930 (for **6**), -651931 (for **7**), -651932 (for **8**), and -651933 (for **9**) contain the supplementary crystallographic data for this paper. These data can be obtained free of charge from The Cambridge Crystallographic Data Center via http://www.ccdc.cam.ac.uk/data_request/cif.

Acknowledgments

This work was supported by the National Natural Science Foundation (No. 20525101), the Natural Science Foundation of Jiangsu Province (No. BK2004205), the Specialized Research Fund for the Doctoral Program of Higher Education (No. 20050285004), and the State Key Laboratory of Coordination Chemistry of Nanjing University and the Qin-Lan Project of Jiangsu Province in China.

[1] R. Robson, B. F. Hoskins, *J. Am. Chem. Soc.* **1990**, *112*, 1546–1554.
[2] P. J. Stang, B. Olenyuk, *Acc. Chem. Res.* **1997**, *30*, 502–518.
[3] F. A. Cotton, C. Lin, C. A. Murillo, *Acc. Chem. Res.* **2001**, *34*, 759–771.
[4] M. Eddaoudi, D. B. Moler, H. L. Li, B. Chen, T. M. Reineke, M. O'Keeffe, O. M. Yaghi, *Acc. Chem. Res.* **2001**, *34*, 319–330.
[5] H. D. Selby, B. K. Roland, Z. P. Zheng, *Acc. Chem. Res.* **2003**, *36*, 933–944.
[6] H. T. Chifotides, K. R. Dunbar, *Acc. Chem. Res.* **2005**, *38*, 146–156.
[7] L. M. C. Beltran, J. R. Long, *Acc. Chem. Res.* **2005**, *38*, 325–334.
[8] Y. V. Mironov, N. G. Naumov, K. A. Brylev, Q. A. Efremova, V. E. Fedorov, K. Hegetschweiler, *Angew. Chem. Int. Ed.* **2004**, *43*, 1297–1300.
[9] Z. H. Yan, C. S. Day, A. Lachgar, *Inorg. Chem.* **2005**, *44*, 4499–4505.
[10] B. F. Abrahams, M. G. Haywood, R. Robson, *Chem. Commun.* **2004**, 938–939.
[11] J. P. Lang, Q. F. Xu, Z. N. Chen, B. F. Abrahams, *J. Am. Chem. Soc.* **2003**, *125*, 12682–12683.
[12] N. B. O'Brien, T. O. Marier, I. C. Paul, R. S. Drago, *J. Am. Chem. Soc.* **1973**, *95*, 6640–6645.
[13] J. P. Costes, J. P. Laurent, J. M. M. Sanchez, J. S. Varela, M. Ahlgren, M. Sundberg, *Inorg. Chem.* **1997**, *36*, 4641–4646.
[14] Z. Q. Xu, L. K. Thompson, C. J. Matthews, D. O. Miller, A. E. Goeta, J. A. K. Howard, *Inorg. Chem.* **2001**, *40*, 2446–2449.
[15] N. M. Shavaleev, Z. R. Bell, G. Accorsi, M. D. Ward, *Inorg. Chim. Acta* **2003**, *351*, 159–166.
[16] X. Z. Li, L. N. Zhu, C. Q. Li, D. Z. Liao, *Inorg. Chem. Commun.* **2006**, *9*, 1297–1300.
[17] Q. M. Wang, X. T. Wu, W. J. Zhang, T. L. Sheng, P. Lin, J. M. Li, *Inorg. Chem.* **1999**, *38*, 2223–2226.
[18] B. Vangdal, J. Carranza, F. Lloret, M. Julve, J. Sletten, *J. Chem. Soc. Dalton Trans.* **2002**, 566–574.
[19] J. Carranza, C. Brennan, J. Sletten, F. Lloret, M. Julve, *J. Chem. Soc. Dalton Trans.* **2002**, 3164–3170.
[20] J. D. Woodward, R. V. Backov, K. A. Abboud, D. Dai, H. J. Koo, M. H. Whangbo, M. W. Meisel, D. R. Talham, *Inorg. Chem.* **2005**, *44*, 638–648.
[21] J. P. Lang, Q. F. Xu, R. X. Yuan, B. F. Abrahams, *Angew. Chem. Int. Ed.* **2004**, *43*, 3917–3921.
[22] J. P. Lang, C. M. Jiao, S. B. Qiao, W. H. Zhang, B. F. Abrahams, *Inorg. Chem.* **2005**, *44*, 3664–3668.
[23] Q. F. Xu, J. X. Chen, W. H. Zhang, Z. G. Ren, H. X. Li, Y. Zhang, J. P. Lang, *Inorg. Chem.* **2006**, *45*, 4055–4064.
[24] J. X. Chen, W. H. Zhang, X. Y. Tang, Z. G. Ren, H. X. Li, Y. Zhang, J. P. Lang, *Inorg. Chem.* **2006**, *46*, 7671–7680.
[25] J. P. Lang, Q. F. Xu, W. H. Zhang, H. X. Li, Z. G. Ren, J. X. Chen, Y. Zhang, *Inorg. Chem.* **2006**, *45*, 10487–10496.
[26] Q. Y. Li, W. H. Zhang, H. X. Li, X. Y. Tang, J. P. Lang, Y. Zhang, X. Y. Wang, G. Song, *Chin. J. Chem.* **2006**, *24*, 1716–1720.
[27] M. A. Halcrow, *Coord. Chem. Rev.* **2005**, *249*, 2880–2908.
[28] G. Zoppellaro, A. Geies, V. Enkelmann, M. Baumgarten, *Eur. J. Org. Chem.* **2004**, 2367–2374.
[29] S. A. Willison, H. Jude, R. M. Antonelli, J. M. Rennekamp, N. A. Eckert, J. A. K. Bauer, W. B. Connick, *Inorg. Chem.* **2004**, *43*, 2548–2555.
[30] N. K. Solanki, E. J. L. McInnes, D. Collison, C. A. Kilner, J. E. Davies, M. A. Halcrow, *J. Chem. Soc. Dalton Trans.* **2002**, 1625–1630.
[31] K. Nakamoto, *Infrared and Raman Spectra of Inorganic and Coordination Compounds, Part B: Applications in Coordination, Organometallic, and Bioinorganic Chemistry*, 5th ed., Wiley, New York, **1997**, pp. 124–126.
[32] A. M. Schuitema, P. G. Aubel, I. A. Koval, M. Engelen, W. L. Driessen, J. Reedijk, M. Lutz, A. L. Spek, *Inorg. Chim. Acta* **2003**, *355*, 374–385.
[33] K. Steiner, W. Willing, U. Müller, K. Dehnicke, *Z. Anorg. Allg. Chem.* **1987**, *55*, 7–15.

[34] J. C. Wasilke, G. Wu, X. H. Bu, G. Kehr, G. Erker, *Organometallics* **2005**, *24*, 4289–4297.
[35] N. Mondal, S. Mitra, V. Gramilich, S. O. Ghodsi, K. M. A. Malik, *Polyhedron* **2001**, *20*, 135–141.
[36] J. Losada, I. Del Peso, L. Beyer, *Inorg. Chim. Acta* **2001**, *321*, 107–115.
[37] S. Torelli, C. Belle, I. Gautier-Luneau, J. L. Pierre, E. Saint-Aman, J. M. Latour, L. L. Pape, D. Luneau, *Inorg. Chem.* **2000**, *39*, 3526–3536.
[38] D. L. Jameson, K. A. Goldsby, *J. Org. Chem.* **1990**, *55*, 4992–4994.
[39] I. Csoregh, P. Kierkegaard, R. Norrestam, *Acta Crystallogr., Sect. B: Struct. Sci.* **1975**, *31*, 314–317.
[40] G. M. Sheldrick, *SHELXS-97and SHELXL-97. Program for the refinement of crystal structures*, University of Göttingen, Germany, **1997**.

Received: June 26, 2007
Published Online: October 17, 2007

